5-27-2004

Data-Model Comparison Search Analysis of Coincident PBO Balmer α, EURD Lyman β Geocoronal Measurements From March 2000

J. Bishop
Naval Research Laboratory

E. J. Mierkiewicz
University of Wisconsin - Madison, mierkiee@erau.edu

F. L. Roesler
University of Wisconsin - Madison

J. F. Gómez
Laboratorio de Astrofí´sica Espacial y Fí´sica Fundamental, INTA

C. Morales
Laboratorio de Astrofí´sica Espacial y Fí´sica Fundamental, INTA

Data-model comparison search analysis of coincident PBO Balmer α, EURD Lyman β geocoronal measurements from March 2000

J. Bishop
E. O. Hulburt Center for Space Research, Naval Research Laboratory, Washington, D. C., USA

E. J. Mierkiewicz and F. L. Roesler
Department of Physics, University of Wisconsin-Madison, Madison, Wisconsin, USA

J. F. Gómez and C. Morales
Laboratorio de Astrofísica Espacial y Física Fundamental, INTA, Madrid, Spain

Received 28 July 2003; revised 3 February 2004; accepted 24 February 2004; published 27 May 2004.

[1] Recent Lyman series and Balmer series airglow measurements provide a fresh opportunity to investigate the density distribution and variability of atomic hydrogen in the upper atmosphere. Dedicated nightside Balmer α Fabry-Perot spectrometer measurements at the Pine Bluff Observatory (PBO), University of Wisconsin-Madison, have been acquired since late 1999 taking advantage of several technological advances. Extreme ultraviolet spectral radiance measurements by the Espectrógrafo Ultravioleta extremo para la Radiación Difusa (EURD) instrument on the Spanish MINISAT-1 satellite from October 1997 to December 2001 provide extensive sets of geocoronal Lyman β, Lyman γ and He 584 Å emission intensities. In this paper, coincident EURD Lyman β and PBO Balmer α radiance measurements from the early March 2000 new moon period are presented. In addition to serving as examples of the data sets now available, the data volume poses an analysis challenge not faced in prior geocoronal studies. A data-model comparison search procedure employing resonance radiation transport results for extensive sets of parametric density distribution models is being developed for use in analyses of multiple large data sets; this is described, and example results for the PBO and EURD March 2000 data sets are presented. The tightness of the constraints obtained for the solar line-center Lyman β irradiance and the atomic hydrogen column abundance is somewhat surprising, given the crudeness of the parameter binning in the search procedure and the fact that a small number of recognized corrections remain to be made to each data set. *INDEX TERMS:* 0310 Atmospheric Composition and Structure: Airglow and aurora; 0355 Atmospheric Composition and Structure: Thermosphere—composition and chemistry; 7837 Space Plasma Physics: Neutral particles; 0394 Atmospheric Composition and Structure: Instruments and techniques; *KEYWORDS:* airglow measurements: Lyman series, Balmer series; airglow analysis: techniques and methods; atmospheric composition: atomic hydrogen; geocoronal density distributions and radiative transport; exospheres

Citation: Bishop, J., E. J. Mierkiewicz, F. L. Roesler, J. F. Gómez, and C. Morales (2004), Data-model comparison search analysis of coincident PBO Balmer α, EURD Lyman β geocoronal measurements from March 2000, *J. Geophys. Res.*, *109*, A05307, doi:10.1029/2003JA010165.

1. Introduction

[2] Determination of the density distribution of atomic hydrogen in the upper atmosphere has remained inconclusive. In situ measurements by mass spectrometers were performed on a number of missions prior to 1983 (e.g., the Atmospheric Explorer series of satellites), but these are indirect and cover a limited altitude range; the atomic hydrogen density [H] itself was not measured but was inferred from [O], [H^+] and [O^+] measurements made by instruments with discrepant calibrations [*Breig et al.*, 1985]. Optical measurements of the Lyman series and Balmer series resonance lines in the airglow have been carried out for several decades [*Meier*, 1991]. Analyses of Lyman α (1216 Å) measurements obtained by satellite-borne instruments have exploited the optically thick character of the apparent column emission rates (ACERs, also referred to as intensities in the following) to obtain estimates of parameters (e.g., the exobase density) applied in vertical distribution density models [*Anderson et al.*, 1987a; *Bush*

0148-0227/04/2003JA010165

and Chakrabarti, 1995; *Bishop*, 2001]. However, analyses of the weak Lyman β (1026 Å) and Balmer α (6563 Å) airglow intensities (the latter measured from ground stations) have in the past yielded significant disagreements with Lyman α results [*Weller et al.*, 1971; *Anderson et al.*, 1987b]. Recent work has shown that, within the context of limited data sets, the apparent discrepancies among in-situ, Lyman α, and Balmer α measurements can be resolved once instrument characteristics, modeling capabilities, and valid empirical input parameters (e.g., solar Lyman series line-center fluxes [*Warren et al.*, 1998]) are given adequate attention [*Bishop*, 2001; *Bishop et al.*, 2001]. It has not been shown, however, that this resolution extends to more general geophysical and solar activity conditions nor how to relate ground-based or thermospheric satellite measurements to observations made deep in the geocorona (e.g., the Lyman α measurements made at geocentric radii above 2 R_E by OGO 5 [*Thomas and Bohlin*, 1972; *Bertaux and Blamont*, 1973], DE-1 [*Rairden et al.*, 1986], and IMAGE/GEO [*Østgaard et al.*, 2003]).

[3] In this paper, coincident Lyman β and Balmer α measurements for the new moon period of early March 2000 are presented to bring attention to the extensive data sets now available and to describe a data-model comparison analysis procedure suitable for analysis of large data sets. The Lyman β data were obtained by the Espectrógrafo Ultravioleta extremo para la Radiación Difusa (EURD) instrument on the Spanish MINISAT-1 satellite that was launched in April 1997 and operated until late 2001 [*García Primo*, 2001]. The Balmer α measurements are from the Pine Bluff Observatory, University of Wisconsin-Madison [*Mierkiewicz et al.*, 1999; *Mierkiewicz*, 2002]. Although each data set must be regarded as preliminary in that recognized data reduction steps remain to be completed, the selected measurements serve as an example of the analysis challenge to be faced in extracting valid parametric descriptions of the atomic hydrogen density distribution. Coincident EURD, PBO measurements covering a number of new moon periods are archived and are expected to be suitable for detailed analysis once the respective data processing steps are completed; in addition, the described analysis procedure can be readily expanded to include coincident PBO Balmer β (4861 Å) measurements, Balmer line data from other ground stations (e.g., WHαM [*Nossal et al.*, 2001]), and detailed, high quality Lyman line data from other satellites (e.g., FUSE [*Feldman et al.*, 2001] and IMAGE/GEO [*Østgaard et al.*, 2003]).

2. March 2000 Measurements

[4] The March 2000 new moon period (29 February to 6 March) was generally quiet (daily Ap > 12 only on 1 March with a value of 21). Solar activity levels remained in the $F_{10.7}$ range 197 (4 March) to 229 (1 March) with an 81-day average value of 182. The globally averaged exobase temperature (T_{exo}) predicted by MSIS [*Hedin*, 1991] for this period is 1197 K, with a globally averaged exobase density ([H](z_{exo})) of 4.3×10^4 cm^{-3}. Little night-to-night variation is seen in either data set.

2.1. PBO Measurements

[5] Balmer α and β data sets have been acquired with a large aperture (15 cm), double etalon, Fabry-Perot annular summing spectrometer dedicated to airglow measurements located at the Pine Bluff Observatory (PBO), University of Wisconsin-Madison (43.07°N, 270.33°E) since 2000 [*Mierkiewicz et al.*, 1999; *Mierkiewicz*, 2002]; a similar instrument, the Wisconsin Hα Mapper (WHαM) primarily used for galactic measurements, has been in operation since 1997 at Kitt Peak, AZ (31.98°N, 248.40°E) [*Nossal et al.*, 2001]. Fabry-Perot spectrometers, with high spectral resolution and high throughput, are well suited for detailed studies of faint diffuse emissions, the former providing separation of the geocoronal emission line from the galactic/interstellar background and enabling detailed line profile studies, the latter providing good signal-to-noise ratios (S/N) needed for capturing emission variations associated with viewing direction, local time and changing atmospheric conditions and for observing very weak emissions (e.g., Balmer β). The annular summing technique images the Fabry-Perot annular fringe pattern onto a low noise, cryogenically cooled charge-coupled device (CCD) with a high quantum efficiency (∼80% at B-α), resulting in a gain in sensitivity of a factor of 10 or more compared with more conventional scanning Fabry-Perots [*Coakley et al.*, 1996]. The PBO Fabry-Perot has an optical field-of-view (FOV) diameter of ∼1.5° and the spectral range at B-α is 75 km/s (∼1.6 Å) at 3.75 km/s (∼0.08 Å) resolution ($R = \lambda/\Delta\lambda \approx 80{,}000$). Typical PBO B-α intensities are in the range 2–15 R, with signal-to-noise ratios of ∼50 for 5–10 minute integrations. On a good night, 20–40 spectra are obtained. Individual measured spectra are reduced using a 4-parameter fit procedure incorporating nine Gaussian line components grouped into two clusters and convolved with the instrument profile, the first cluster containing the two fine structure lines directly excited by Lyman β scattering with a fixed 2-to-1 emission ratio and the second cluster containing the full set of fine structure lines set in line ratios given in *Meier* [1995]; the four free parameters are thus the intensities for each of the two clusters, the emission line width common to all the fine-structure lines, and the spectral position. Absolute intensity calibrations are based on same-night observations, when possible, of well-established nebular emission sources (e.g., the North American Nebula). The PBO intensity data for the March 2000 new moon period are shown in Figure 1.

2.2. EURD Measurements

[6] The EURD instrument on the Spanish satellite MINISAT-1 carried out measurements of the diffuse interstellar extreme ultraviolet (350–1100 Å) radiance from October 1997 to December 2001. Satellite launch occurred 21 April 1997 on a Pegasus vehicle from Gran Canaria Island [*García Primo*, 2001]; the orbit was roughly circular at ∼570 km altitude and 151° inclination. A detailed description of the instrument, a collaboration of the Spanish Instituto Nacional de Técnica Aeroespacial and the Center for EUV Astrophysics, University of California, Berkeley, is given by *Bowyer et al.* [1997]. Two spectrometers were employed, covering spectral intervals 350–900 Å ("short wavelength" or SW spectrometer) and 550–1100 Å ("long wavelength" or LW spectrometer), each at ∼6 Å spectral resolution. EURD pointing was in the antisolar direction, with data acquired during the nightside transits in a repeating exposure sequence (30 s open aperture exposures in a

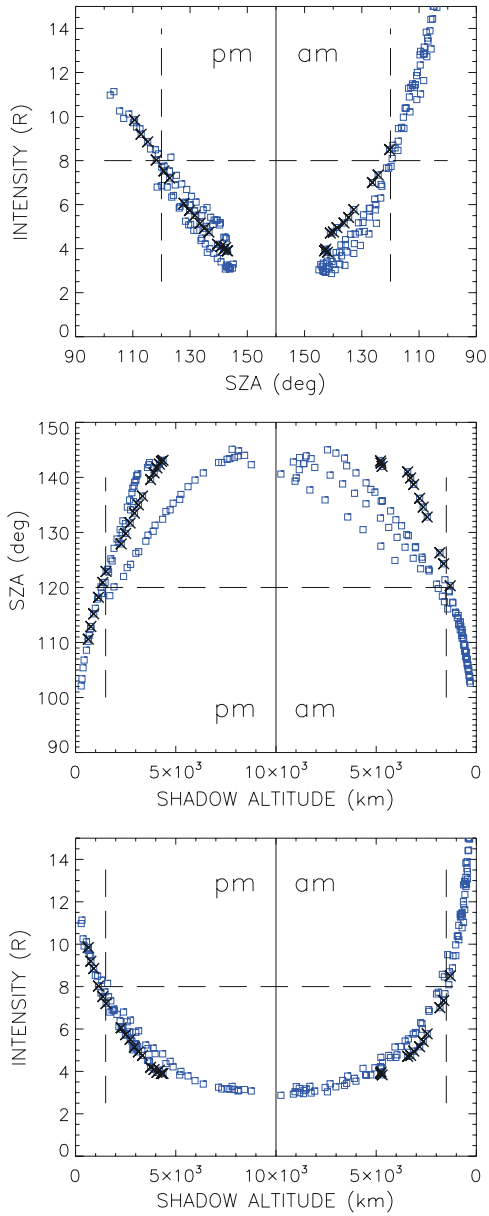

Figure 1. PBO viewing directions and Balmer α intensities for the nights of 28 February and 2–6 March 2000 (blue squares); data from the night of 4 March 2000 are identified by the times symbol (×). (top) Intensities versus PBO solar zenith angle (SZA). Different viewing sequences were followed each night. Corrections for galactic emission and tropospheric scattering have not been made. (middle) PBO SZA versus LOS shadow altitude for each intensity measurement, showing the LOS pointing sequences associated with viewing different positions within regions of low galactic background. Shadow altitude is the altitude of the point where a nightside line of sight from a ground station exits the planetary shadow cylinder defined by the resonant radiation "black level" altitude at the terminator (102 km for Lyman β). (bottom) Intensities versus LOS shadow altitudes. Comparison with the top panel shows LOS shadow altitude to be the more advantageous independent parameter.

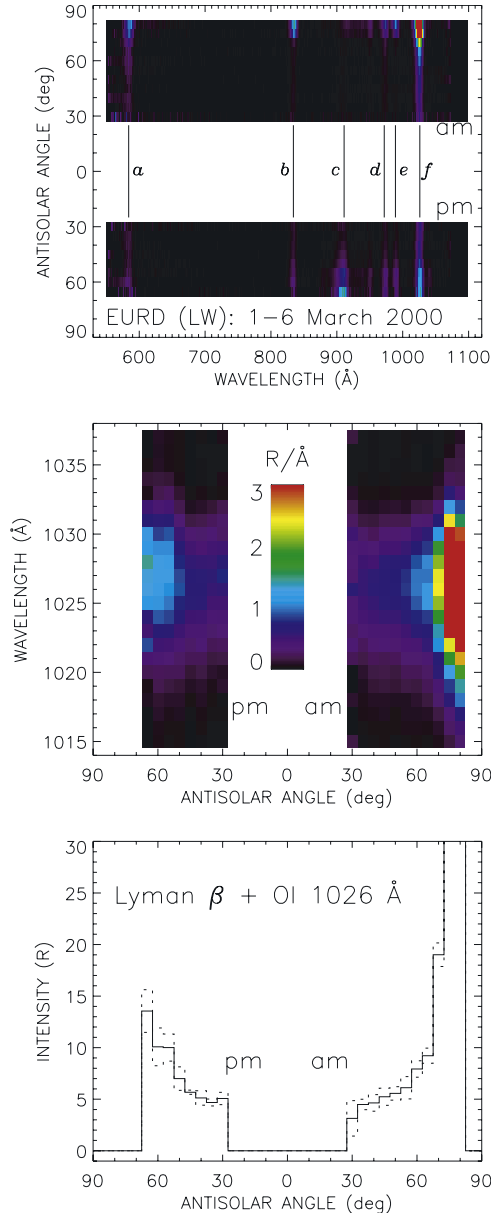

Figure 2. (top) EURD long-wavelength spectrometer antisolar radiance data from 1 to 6 March 2000. Airglow lines of interest are a: He 584 Å, b: O^+ 834 Å, c: $O^+ + e^-$ 911 Å continuum, d: H Ly-γ 972 Å, e: OI 989 Å sextuplet, and f: H Ly-β + OI 1026 Å. (middle) 1026 Å spectral region; color saturation near the dawnside terminator is from OI 1026 Å sextuplet emission. (bottom) Derived Ly-β + OI 1026 Å intensities versus antisolar angle (ASA) bin; dashed histograms display uncertainty range associated with uncertainties in preliminary background estimates.

90 s cycle). The field of view was 25° × 8° (approximated as an angular box in this study); because of this, the data from near-terminator locations show strong contributions from atomic oxygen (e.g., the OI 1026 Å sextuplet). LW data for the 1–6 March 2000 period are shown in Figure 2, with the spectra obtained in each 5° bin of spacecraft position angle with respect to the antisolar direction (antisolar angle or ASA) averaged (top panel) and corrected

Table 1. Parameter Grids

Parameter	Grid Values	Units	Definition
n_{exo}	2, 2.8, 4, 5.7, 8, 11.3 × 10^4	cm^{-3}	exobase density (494 km)
φ	0.3, 1, 3, 9 × 10^8	cm^{-2} s^{-1}	photochemical upward flux
n_{max}	0.3, 1, 3, 9 × 10^8	cm^{-3}	mesospheric peak density (85 km)
T_s	450, 600, 750, 1100	K	satellite atom KDF parameter[a]
$f(n_s)$	0.73, 1, 1.36	-	n_s scaling
$f(F_{10.7})$	0.85, 1, 1.15	-	daily $F_{10.7}$ scaling[b]

[a]Associated n_s values: 3 × 10^7, 2.2 × 10^6, 5 × 10^5, 7.4 × 10^4 cm^{-3}, respectively.

[b]Mean value for the early March 2000 daily $F_{10.7}$ index is 211; corresponding mean MSIS exobase temperature (T_{exo}), atomic hydrogen density ([H] (z_{exo})) values for the evening and predawn sectors are 1257 K, 4.1 × 10^4 cm^{-3} and 1067 K, 5.9 × 10^4 cm^{-3}, respectively.

for estimated instrumental background in the vicinity of Lyman β (middle and bottom panels). Detector sensitivity within the FOV box has been modeled as a factor-of-two triangular variation with respect to the angular displacement along the 25°-wide viewing direction. Further information regarding the spacecraft mission and the EURD instrument is provided by *Edelstein et al.* [2001] and *Gómez et al.* [2001]. Absolute calibration is discussed by *Morales et al.* [2000, 2001], with in-flight calibration in the 911–1100 Å wavelength interval based on α Vir (Spica, HD 116658) and other bright B star spectrum measurements. A preliminary description of the nightside airglow as seen by EURD is given by *López-Moreno et al.* [1998].

3. Analysis

3.1. Data-Model Comparison Search Procedure

[7] The observed ACERs relate to the underlying atomic hydrogen density distribution via resonance scattering. Atomic hydrogen column densities above 100 km are large enough that Lyman β multiple scattering needs to be taken into account, particularly in quantitative analysis of nightside data where scattering within the shadow provides an appreciable fraction of the fluorescence intensities seen from ground stations. O_2 photoabsorption dominates below 102 km altitude, defining the lower boundary or "black level" z_b for Ly-β volume emission rates. Given the uncertainties in [H](z) and the solar Lyman β line-center flux associated with older data sets, coupled with the large volume of data now available, a parametric model search procedure is being developed. The resonance radiation transport algorithm lyao_rt [*Bishop*, 1999, 2001] has been employed to generate extensive sets of Lyman β source functions for each nightside sector (evening and predawn), which are then applied in simulations of the PBO B-α and EURD Ly-β measurements. In this initial trial, [H] distributions and background model atmospheres specified by six parameters (Table 1) define the scattering environment in each sector. The [H](z) thermospheric parameters n_{exo}, φ and n_{max} are discussed in *Bishop* [2001] and the satellite component parameters T_s, n_s in *Bishop* [1991]; MSIS background atmospheres in each sector are set by the mean geophysical conditions described earlier with an additional scaling factor applied to mean daily $F_{10.7}$ specifying the thermospheric temperature profile. In all, 3456 Lyman β scattering models are generated, catalogued and archived separately for each nightside sector (evaluated at locations ~20° behind the respective terminators). Corresponding sets of line-of-sight (LOS) ACER integrations are then performed, catalogued and archived for the observation locations and viewing directions of the measurements made by each instrument within each sector, assuming a unit incident solar line-center flux ($\pi\mathcal{F}_\circ$). The EURD FOV has been modeled using multiple lines of sight contained within a simple angular box centered on each nominal ASA LOS and the calculated Ly-β ACERs averaged with weighting based on the instrument sensitivity distribution previously described; single LOS B-α ACER calculations are made for each PBO intensity measurement. The $\pi\mathcal{F}_\circ$ magnitudes required to fit the measured PBO and EURD intensities in each nightside sector are then set by the data points near 3000 km shadow altitude and in the 40° ASA bins, respectively, after correction estimates have been applied (described below).

[8] Given a parametric model database like the one just described, direct data-model comparisons can be carried out to find candidate "solutions" (e.g., parameter combinations yielding self-consistent data-model fits for both instruments). In the search scheme settled upon in this trial, the n_{exo}, φ and n_{max} parameters and the $F_{10.7}$ scaling factor for each sector are considered independent but the satellite component T_s, n_s parameters are shared. The mesospheric density parameter (n_{max}), which specifies the atomic hydrogen densities at altitudes below 120 km, has the weakest impact on the modeling in this study. While the mesospheric [H] distribution can have an appreciable impact on dayside Ly-α intensities [*Bishop*, 2001], the Ly-β black level is high enough that the rapid density increase with decreasing altitude below 120 km has little direct impact on B-α intensities as seen from ground stations or on upward viewing Ly-β intensities obtained near the exobase. Hence, in this initial study, n_{max} has been set to 1 × 10^8 cm^{-3} (MSIS values are in the range 1–1.5 × 10^8 cm^{-3}). This simplification nevertheless leaves a total of $6^2 \times 4^2 \times 4 \times 3 \times 3^2$ or 62,208 predawn, evening source function pairings to evaluate. The trial search criteria settled on are:

[9] 1. solar Ly-β line-center fluxes for both data sets must be in the range 6–18 × 10^9 ph cm^{-2} s^{-1} $Å^{-1}$;

[10] 2. the predawn, evening $\pi\mathcal{F}_\circ$ values for each data set taken alone cannot differ by more than 20%;

[11] 3. the average of the PBO predawn, evening $\pi\mathcal{F}_\circ$ values cannot differ from the averaged EURD value by more than 30%;

[12] 4. the predawn, evening vertical column densities above 102 km ($\mathcal{N}_b$) cannot differ by more than 50%; and

[13] 5. $n_{exo}(PM) < n_{exo}(AM)$.

[14] The first criterion simply requires that the implied solar line-center Ly-β fluxes lie within a range of reasonable $\pi\mathcal{F}_\circ$ values, taking into account the absolute intensity calibration uncertainties stated for each instrument (~10%

for PBO B-α, ~30% for EURD at Ly-β); for reference, extrapolation of the solar EUV rocket measurements of *Woods et al.* [1998] combined with the assumption that the SOHO/SUMER solar Ly-β line profile under quiet conditions [*Warren et al.*, 1998] remains valid under active conditions ($F_{10.7} \approx 210$) gives $\pi\mathcal{F}_\circ$ values of $9-12 \times 10^9$ ph cm^{-2} s^{-1}. Given the crudeness of the parameter gridding and the data-modeling limitations discussed below, however, tighter ranges in $\pi\mathcal{F}_\circ$ in criteria 2 and 3 cannot be enforced; for example, predawn, evening differences in the tropospheric scattering correction of the PBO data or in the local interstellar medium (LISM) Ly-β contribution to the EURD data must be allowed for in criterion 2 and calibration offsets between the two instruments must be allowed for in criterion 3. Taken together, criteria 1–3 addressing the incident line-center solar flux eliminate a large fraction (>98%) of the solution candidates (i.e., source function pairings); it is worth noting that all candidate solutions with $n_{exo} > 8 \times 10^4$ cm^{-3} in either sector have been removed at this stage. Criterion 4 reflects a simple expectation that while upper thermospheric, lower exospheric densities may vary diurnally by up to a factor of ~3, appreciably smaller variations are expected in the lower thermosphere and out in the exosphere proper ($R > 1.5$ R_E). Criterion 5 is based on past data analyses [*Breig et al.*, 1985; *Bishop et al.*, 2001] showing n_{exo} dawn-dusk ratios are expected to be in the range 2–2.5; this is considered sufficiently larger than the n_{exo} gridding factor ($\sqrt{2}$) to remain valid when other data-model uncertainties are taken into account. The final number of reasonable solutions is 52. An additional constraint had been applied, that given the clearly captured intensity variation with respect to solar zenith angle seen in the 4 March 2000 data, the PBO-lyao_rt ACER ratios at 1500 km and 5000 km shadow altitude cannot differ from unity by more than 20%, but this led to no additional elimination of candidate solutions. Examples of search results are shown in Figure 3.

3.2. Data Modeling Limitations

[15] While the instrumental resolution and NAN-based calibrations provide confidence in the PBO data, there are several factors not yet taken into account in conversion to physical units, e.g., cascade enhancement and tropospheric scattering. The main consequence of cascade is modification of the B-α emission line profile with a contribution to total intensity of ~6–10% [*Meier*, 1995; *Nossal et al.*, 1998]; same-night measurements of Balmer β and Balmer α have been made both at PBO and at Kitt Peak with the WHαM instrument that will provide a reassessment of cascade in the geocoronal emission once data reduction is completed. Tropospheric scattering constitutes another net enhancement [*Leinert et al.*, 1998; *Hong et al.*, 1998] that was given close attention in the University of Wisconsin B-α measurements of *Shih et al.* [1985]. Most measurements by PBO in the March 2000 new moon period (Figure 1) were obtained at observation zenith angles exceeding 20° with relative solar azimuths in the midnight sector (>120°), within a region of low galactic emission. To reduce the impact of tropospheric scattering enhancement uncertainties, this preliminary analysis has centered on the near-zenith data obtained on 4 March 2000 and identified in Figure 1. Overall, the net enhancement in the 4 March 2000 data is expected to be in the 8–20% range; in this trial, a reduction of 14% has been applied.

[16] Similarly, given the ~6 Å resolution, the interplanetary (IP) and interstellar (LISM) Ly-β background in the EURD data must be taken into account. However, direct IP + LISM data are sparse; where available, the intensity measurements are typically expressed in terms of intensity ratios against the more extensively measured Ly-α IP + LISM background [*Murthy et al.*, 1999; *Shemansky et al.*, 1984; *Hord et al.*, 1991]. Directional variations in IP + LISM intensities have not been treated in this preliminary study; combined with uncertainties in Lyman α LISM intensity magnitudes, a crude estimate of 0.5 R (with a factor of ~2 uncertainty) for the Lyman β background has been subtracted from the EURD 1026 Å intensities.

4. Example Results and Discussion

[17] Since the PBO and EURD data sets are still undergoing reduction, and given the crudeness of the parameter binning applied in the search procedure, definitive results for [H](z) are not being presented. The PBO and EURD viewing schemes are roughly similar (pointing is in the upper hemisphere with respect to zenith, with no limb scanning or disk viewing by EURD); coupled with the fact that except near terminator EURD views only the exosphere whereas PBO measurements involve the total thermosphere + exosphere column abundance, it might be expected that a wide range of candidate solutions will satisfy the search criteria applied in this initial trial. The small number of source function pairings retrieved in the search is encouraging and somewhat surprising. None have predawn, evening n_{exo} parameters that are not adjacent and most candidate solutions have predawn, evening variations in T_{exo} larger than predicted by MSIS ($f(F_{10.7}) = 1.15$ for the evening sector with $T_{exo} = 1293$ K, $f(F_{10.7}) = 0.85$ with $T_{exo} = 1023$ K for the predawn sector). Most also require "cooler" T_s satellite parameter values ($T_s \leq 750$ K) than associated with a simple evaporative exosphere model, with "enhanced" n_s values ($f(n_s) = 1.4$) [*Bishop*, 1991]; however, the T_s, n_s parameter pairs adopted in this trial are taken from the STP 78-1 dayside data analysis of *Bishop* [1999], which admittedly does not constitute a firm basis for the respective parameter grid spacings and ranges in Table 1.

[18] Four solution examples are shown in Figure 3. Source function pairings a, b, and c are a sequence with decreasing n_{exo} values and $\varphi = 3 \times 10^8$ cm^{-2} s^{-1} in both nightside sectors; pairing d is the same as b except the dawnside φ value is smaller (1×10^8 cm^{-2} s^{-1}). Figure 4 shows the corresponding [H](z) altitude profiles compared with MSIS profiles for the early March 2000 conditions at thermospheric altitudes (102 km < z < 494 km) extended into the exosphere under two simple approximations. Final selection of examples a–d is based on data-model agreement at shadow altitudes near 500 km for the PBO data and at 70° ASA for the EURD data. The overall best fit is solution a, based on the very good fits to the PBO intensities versus shadow altitude (well within the error bars in both sectors) while requiring solar line-center Ly-β fluxes in reasonable agreement with values expected from recent solar measurements (discussed further below). For this solution, exobase densities are close to the MSIS values (5.9×10^4

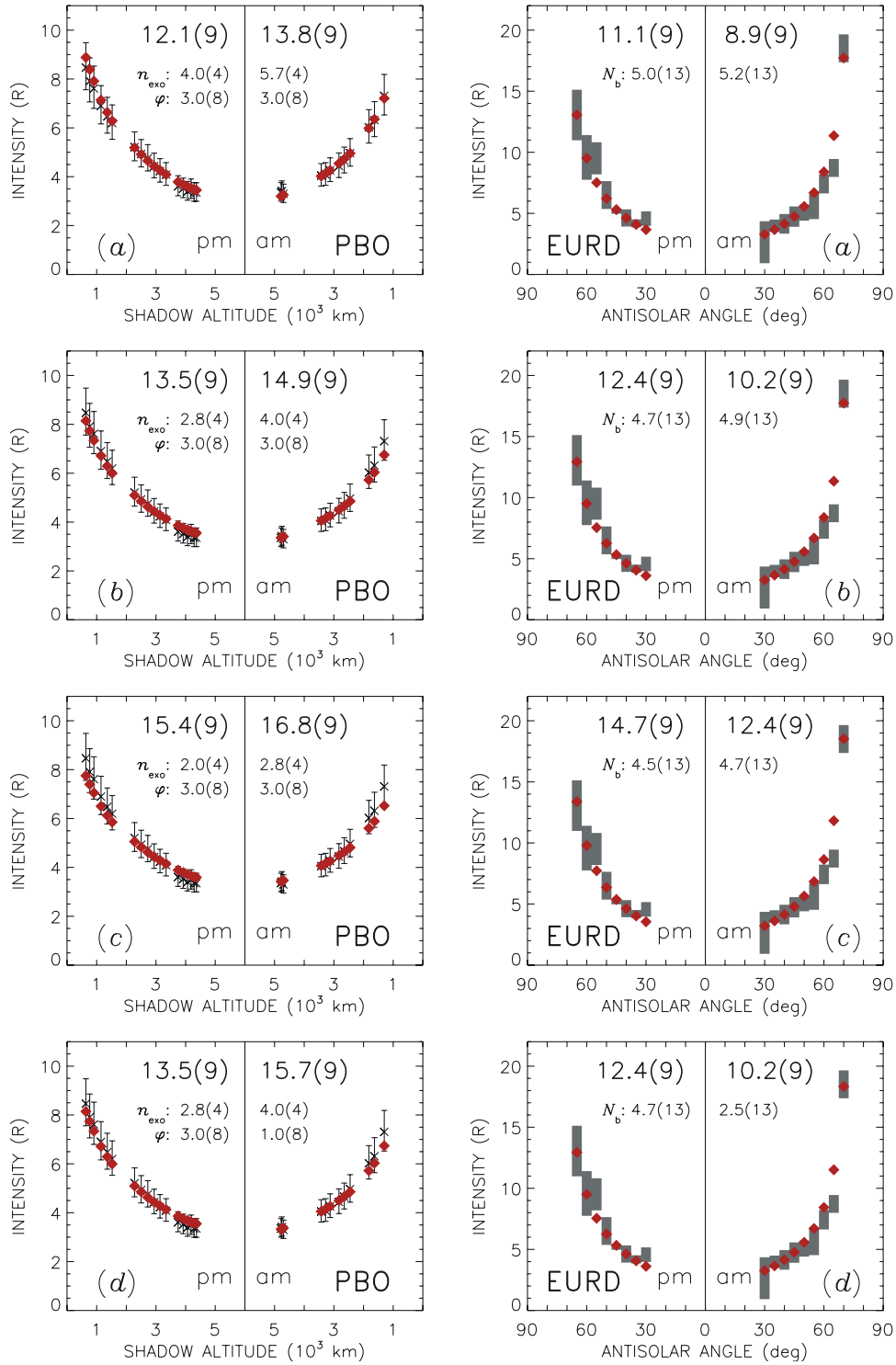

Figure 3. Examples of candidate solutions from the search procedure described in the text. Four examples are shown, with the 4 March 2000 PBO data, lyao_rt model (red diamond) ACER profiles versus LOS shadow altitude in the left-side panels and the 1–6 March 2000 EURD data, lyao_rt model FOV-averaged (red diamond) ACER profiles versus satellite antisolar angle in the right-side panels. Search parameter values for n_{exo} and φ are given in the PBO panels, vertical column densities above 102 km ($\mathcal{N}_b$) are given in the EURD panels. Other parameters: T_s, n_s = 600 K, 3.0×10^6 cm^{-3} for solution a, 750 K, 6.8×10^5 cm^{-3} for solutions b–d; T_{exo} = 1293 K in the evening sector ("pm"), 1023 K in the predawn sector ("am") in all solutions shown. Of the 52 candidate solutions obtained in this trial, solution a provides the best overall fit to both data sets; solutions b–d illustrate the sensitivity of the search procedure to the more effectual parameters. (Note: quantities like 3×10^8 are displayed as "3.0(8)".)

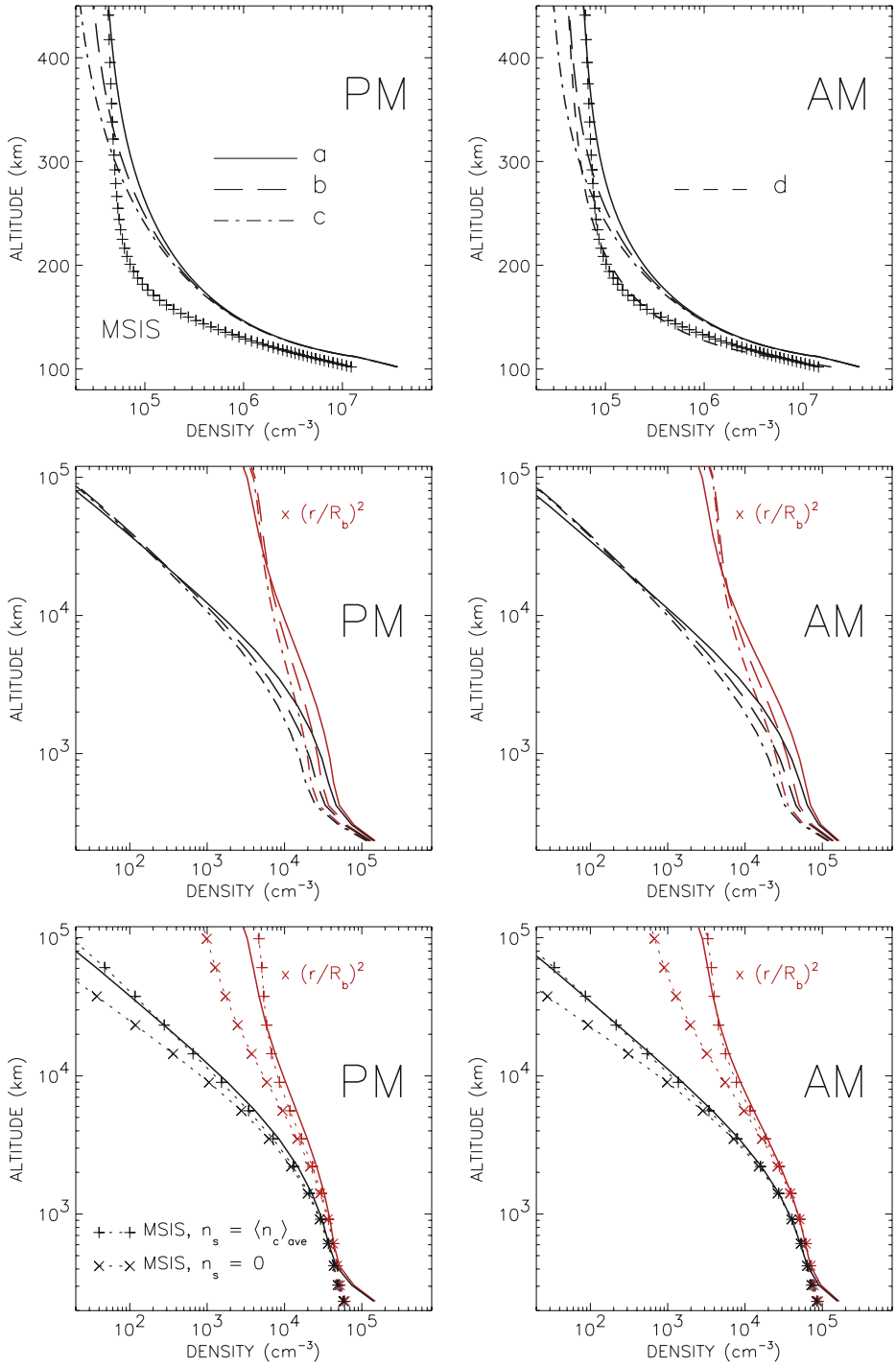

Figure 4. [H](z) profiles for the candidate solutions of Figure 3. Top panels: Thermospheric density profiles for solutions a–d and profiles predicted by MSISE-90 for early March 2000 conditions. Middle panels: Complete density profiles for solutions a–d. [H](z) × $(r/R_b)^2$ profiles (red curves) are also given, showing the radial bin volume content relative to the lower radial boundary (R_b). This radial weighting of [H](z) is not used in lyao_rt calculations but is shown here to convey the impact of the spatial distribution (spherical versus plane-parallel) in the modeling: the decrease in [H](z) with increasing altitude is partially offset by the increase in relative volume to which these densities apply in carrying out the radiative transport calculations. Bottom panels: Comparison of complete density profiles for solution a (solid curves) and two MSIS-based profiles (no satellite atoms and an evaporative satellite distribution), indicating the increasing significance of the satellite atom distribution with increasing altitude.

and 4.1×10^4 cm^{-3} for the predawn and evening sectors, resp.) but the column abundances are considerably larger than the corresponding MSIS values (2.8×10^{13} and 2.3×10^{13} cm^{-2}, resp., with the evaporative satellite component approximation). The predawn atomic hydrogen density profiles of solution d and MSIS, in contrast, have roughly the same distribution below 250 km and total column abundance, but fitting of the PBO and EURD data together requires n_{exo} appreciably smaller than predicted by MSIS and $\pi\mathcal{F}_\circ$ larger than required in solution a. Of the remaining candidate solutions, over half have $\varphi = 9 \times 10^8$ cm^{-2} s^{-1} and $\mathcal{N}_b > 10^{14}$ cm^{-2} in both sectors, with no solutions having $\varphi = 9 \times 10^8$ cm^{-2} s^{-1} in one sector and $\varphi < 9 \times 10^8$ cm^{-2} s^{-1} in the other. These convey the same point evident in Figures 3 and 4, that the correction for diffusive flow required to fit the PBO + EURD data results in a considerable increase of the thermospheric atomic hydrogen content compared with MSIS, but upward fluxes of this magnitude applied in a 1-D profile model are not expected to be realistic (at least not at low latitudes to midlatitudes [see, e.g., *Breig and Hanson*, 1991; *Yung et al.*, 1989]).

[19] In addition to the thermospheric atomic hydrogen content, the column abundance $\mathcal{N}(z_{exo})$ above the exobase needed to fit the EURD data once the thermospheric multiple scattering enhancement has been constrained by the PBO data shows that an appreciable satellite atom component (specified by the T_s, n_s parameters in the analytic [H](z) model) is required. The significance of the satellite atom density distribution is illustrated by the density profiles scaled by $(r/R_b)^2$ in Figure 4. From the perspective of observations made near the planet (e.g., from ground stations or from thermospheric altitudes), it is the content of radial volume elements defined with respect to the lower boundary, rather than density per se, that determines radiative transport (i.e., scattering) radiance contributions from the middle and outer geocorona. The exospheric content at altitudes above $\sim 10^4$ km among the candidate solutions is roughly the same, irrespective of the n_{exo} differences; in fact, [H](z) at altitudes above 20,000 km is larger for solutions b–d than for solution a, having more extended satellite atom distributions compensating for the larger atomic hydrogen densities of solution a at lower altitudes while continuing to satisfy the PBO data criteria described earlier.

[20] There is a factor of 2 variation among the $\pi\mathcal{F}_\circ$ fitting factors for the Figure 3 solutions, from 8.9×10^9 ph cm^{-2} s^{-1} Å^{-1} for the dawnside EURD fit of solution a to 16.8×10^9 ph cm^{-2} s^{-1} Å^{-1} for the dawnside PBO fit of solution c, but within a given source function pairing the range in values is less than 40%. The PBO and EURD predawn, evening values all differ in the same manner, suggesting that differences in the respective correction factors (e.g., tropospheric scattering for PBO B-α, LISM background for EURD Ly-β) between the predawn and evening sectors may be partly responsible. Still, the required solar line-center flux values for most candidate solutions (but not, perhaps, for solution a) are more than a factor of 2 larger than the SOHO/SUMER solar minimum value of 5.1×10^9 ph cm^{-2} s^{-1} Å^{-1} from *Warren et al.* [1998]. A factor of 2 variation of the line-integrated Ly-β flux ($\pi\mathcal{F}$) with respect to solar activity is the maximum variation expected in current empirical solar EUV models [*Lean et al.*, 2003], so a larger variation in the line-center flux requires the solar irradiance (disk-integrated) Ly-β line profile to vary with solar activity. However, direct determinations of $\pi\mathcal{F}_\circ$ under active solar conditions from high spectral resolution measurements are not yet available and it may be that a solar cycle variation in the solar Ly-β irradiance line profile is real.

[21] More detailed analyses can be carried out once several remaining data processing and simulation issues are resolved. However, the solution examples in Figures 3 and 4 clearly show that exobase density alone as a parameter is inadequate in analysis of optical data; fitting of both the PBO and EURD data sets requires specification of [H](z) from ~140 km out to beyond 4 R_E and hence the vertical flux of atomic hydrogen in the thermosphere and the geocoronal satellite atom population must be taken into account on par with n_{exo}. This initial application of the search procedure also shows that column abundances and solar line-center fluxes are the primary quantities that can be directly retrieved from the EURD, PBO data. Once estimates for the remaining data correction factors are resolved, finer gridding of the parameters can be applied and the required solar line-center fluxes assessed against available direct and indirect $\pi\mathcal{F}_\circ$ and $\pi\mathcal{F}$ determinations. Tighter constraints on $\pi\mathcal{F}_\circ$ will narrow the selection results for $\mathcal{N}_b$; however, it cannot be claimed as yet that the number of candidate solutions and associated n_{exo}, φ and T_s, n_s parameter subsets will be reduced to the point of offering a ''unique'' solution for the early March 2000 period. Nevertheless, similar analyses of the PBO + EURD data from other periods are expected to map out atomic hydrogen column abundances and its variation with season and solar cycle variation (the latter through application of the data-model comparison search procedure to coincident EURD and 1997–2001 WHαM data [*Nossal et al.*, 2001]).

[22] **Acknowledgments.** Partial support for J. Bishop is from the Office of Naval Research. NSF support to the University of Wisconsin for E. Mierkiewicz and F. L. Roesler was provided through grants ATM-9908775 and ATM-0228465. J. F. Gómez and C. Morales acknowledge support from MCyT grant AYA 2000-0912 (Spain). The authors would like to thank Susan Nossal and Ron Reynolds for their contributions regarding the PBO data.

[23] Arthur Richmond thanks Seung Soo Hong and N. Østgaard for their assistance in evaluating this paper.

References

Anderson, D. E., Jr., L. J. Paxton, R. P. McCoy, R. R. Meier, and S. Chakrabarti (1987a), Atomic hydrogen and solar Lyman alpha flux deduced from STP 78-1 UV observations, *J. Geophys. Res.*, *92*, 8759–8766.

Anderson, D. E., Jr., R. R. Meier, R. R. Hodges Jr., and B. A. Tinsley (1987b), Hydrogen Balmer alpha intensity distributions and line profiles from multiple scattering theory using realistic geocoronal models, *J. Geophys. Res.*, *92*, 7619–7642.

Bertaux, J. L., and J. E. Blamont (1973), Interpretation of Ogo 5 Lyman alpha measurements in the upper geocorona, *J. Geophys. Res.*, *78*, 80–91.

Bishop, J. (1991), Analytic exosphere models for geocoronal applications, *Planet. Space Sci.*, *39*, 885–893.

Bishop, J. (1999), Transport of resonant atomic hydrogen emissions in the thermosphere and geocorona: Model description and applications, *J. Quant. Spectrosc. Radiat. Transfer*, *61*, 473–491.

Bishop, J. (2001), Thermospheric atomic hydrogen densities and fluxes from dayside Lyman α measurements, *J. Atmos. Sol. Terr. Phys.*, *63*, 331–340.

Bishop, J., J. Harlander, S. Nossal, and F. L. Roesler (2001), Analysis of Balmer α intensity measurements near solar minimum, *J. Atmos. Sol. Terr. Phys.*, *63*, 341–353.

Bowyer, S., J. Edelstein, and M. Lampton (1997), Very high sensitivity extreme ultraviolet spectrometer for diffuse radiation, *Astrophys. J.*, *485*, 523–532.

Breig, E. L., and W. B. Hanson (1991), Deuterium and hydrogen flows in the thermosphere, *J. Geophys. Res.*, *96*, 17,779–17,792.

Breig, E. L., S. Sanatani, and W. B. Hanson (1985), Thermospheric hydrogen: The long-term solar influence, *J. Geophys. Res.*, *90*, 5247–5260.

Bush, B. C., and S. Chakrabarti (1995), Analysis of Lyman α and He I 584-Å airglow measurements using a spherical radiative transfer model, *J. Geophys. Res.*, *100*, 19,609–19,625.

Coakley, M. M., F. L. Roesler, R. J. Reynolds, and S. Nossal (1996), Fabry-Perot CCD annular-summing spectroscopy: Study and implementation for aeronomy applications, *Appl. Opt.*, *35*, 6479–6493.

Edelstein, J., S. Bowyer, E. J. Korpela, M. Lampton, J. Trapero, J. F. Gómez, C. Morales, and V. Orozco (2001), EURD observations of interstellar radiation, *Astrophys. Space Sci.*, *276*, 177–185.

Feldman, P. D., D. J. Sahnow, J. W. Kruk, E. M. Murphy, and H. W. Moos (2001), High-resolution FUV spectroscopy of the terrestrial day airglow with the Far Ultraviolet Spectroscopic Explorer, *J. Geophys. Res.*, *106*, 8119–8129.

García Primo, M. A. (2001), Spanish MINISAT program: Objectives and operational results, *Astrophys. Space Sci.*, *276*, 3–12.

Gómez, J. F., J. Trapero, C. Morales, V. Orozco, J. Edelstein, E. Korpela, and M. Lampton (2001), EURD data processing, *Astrophys. Space Sci.*, *276*, 233–238.

Hedin, A. E. (1991), Extension of the MSIS thermosphere model into the middle and lower atmosphere, *J. Geophys. Res.*, *96*, 1159–1172.

Hong, S. S., S. M. Kwon, Y.-S. Park, and C. Park (1998), Transfer of diffuse astronomical light and airglow in scattering Earth atmosphere, *Earth Planets Space*, *50*, 487–491.

Hord, C. W., et al. (1991), Galileo ultraviolet spectrometer experiment: Initial Venus and interplanetary cruise results, *Science*, *253*, 1548–1550.

Lean, J., H. P. Warren, J. T. Mariska, and J. Bishop (2003), A new model of solar EUV irradiance variability: 2. Comparisons with empirical models and observations and implications for space weather, *J. Geophys. Res.*, *108*(A2), 1059, doi:10.1029/2001JA009238.

Leinert, C., et al. (1998), The 1997 reference of diffuse night sky brightness, *Astron. Astrophys. Suppl. Ser.*, *127*, 1–99.

López-Moreno, J. J., C. Morales, J. F. Gómez, J. Trapero, S. Bowyer, J. Edelstein, M. Lampton, and E. J. Korpela (1998), EURD observations of EUV nightime airglow lines, *Geophys. Res. Lett.*, *25*, 2937–2940.

Meier, R. R. (1991), Ultraviolet spectroscopy and remote sensing of the upper atmosphere, *Space Sci. Rev.*, *58*, 1–185.

Meier, R. R. (1995), Solar Lyman series line profiles and atomic hydrogen excitation rates, *Astrophys. J.*, *452*, 462–471.

Mierkiewicz, E. J. (2002), Fabry-Perot observations of the hydrogen geocorona, dissertation, 213 pp., Univ. of Wisconsin-Madison, Madison.

Mierkiewicz, E. J., F. L. Roesler, J. Bishop, and S. M. Nossal (1999), A systematic program for ground-based Fabry-Perot observations of the neutral hydrogen exosphere, *Proc. SPIE Int. Soc. Opt. Eng.*, *3756*, 323–336.

Morales, C., et al. (2000), Far-ultraviolet absolute flux of α Virginis, *Astrophys. J.*, *530*, 403–407.

Morales, C., et al. (2001), Far-ultraviolet spectra of B stars near the ecliptic, *Astrophys. J.*, *552*, 278–288.

Murthy, J., D. Hall, M. Earl, R. C. Henry, and J. B. Holberg (1999), An analysis of 17 years of Voyager observations of the diffuse far-ultraviolet radiation field, *Astrophys. J.*, *522*, 904–914.

Nossal, S., F. L. Roesler, and M. M. Coakley (1998), Cascade excitation in the geocoronal hydrogen Balmer α line, *J. Geophys. Res.*, *103*, 381–390.

Nossal, S., F. L. Roesler, J. Bishop, R. J. Reynolds, M. Haffner, S. Tufte, J. Percival, and E. J. Mierkiewicz (2001), Geocoronal Hα intensity measurements using the Wisconsin Hα Mapper Fabry-Perot facility, *J. Geophys. Res.*, *106*, 5605–5616.

Østgaard, N., S. B. Mende, H. U. Frey, G. R. Gladstone, and H. Lauche (2003), Neutral hydrogen density profiles derived from geocoronal imaging, *J. Geophys. Res.*, *108*(A7), 1300, doi:10.1029/2002JA009749.

Rairden, R. L., L. A. Frank, and J. D. Craven (1986), Geocoronal imaging with Dynamics Explorer, *J. Geophys. Res.*, *91*, 13,613–13,630.

Shemansky, D. E., D. L. Judge, and J. M. Jessen (1984), Pioneer 10 and Voyager observations of the interstellar medium in scattered emission of the He 584 Å and H Lyα 1216 Å lines, in *IAU Colloquium 81, Local Interstellar Medium*, edited by Y. Kondo, F. C. Bruhweiler, and B. D. Savage, *NASA Conf. Publ.*, *NASA CP-2354*, 24–27.

Shih, P., F. L. Roesler, and F. Scherb (1985), Intensity variations of geocoronal Balmer alpha emission, 1. Observational results, *J. Geophys. Res.*, *90*, 477–490.

Thomas, G. E., and R. C. Bohlin (1972), Lyman-alpha measurements of neutral hydrogen in the outer geocorona and in interplanetary space, *J. Geophys. Res.*, *77*, 2752–2761.

Warren, H. P., J. T. Mariska, and K. Wilhelm (1998), High-resolution observations of the solar hydrogen Lyman lines in the quiet sun with the SUMER instrument on *SOHO*, *Astrophys. J. Suppl. Ser.*, *119*, 105–120.

Weller, C. S., R. R. Meier, and B. A. Tinsley (1971), Simultaneous measurements of the hydrogen airglow emissions of Lyman alpha, Lyman beta, and Balmer alpha, *J. Geophys. Res.*, *76*, 7734–7744.

Woods, T. N., G. J. Rottman, S. M. Bailey, S. C. Solomon, and J. R. Worden (1998), Solar extreme ultraviolet irradiance measurements during solar cycle 22, *Sol. Phys.*, *177*, 133–146.

Yung, Y. L., J.-S. Wen, J. I. Moses, B. M. Landry, M. Allen, and K.-J. Hsu (1989), Hydrogen and deuterium loss from the terrestrial atmosphere: A quantitative assessment of nonthermal escape fluxes, *J. Geophys. Res.*, *94*, 14,971–14,989.

J. Bishop, E. O. Hulburt Center for Space Research, Naval Research Laboratory, Code 7643, 4555 Overlook Avenue, SW, Washington, D. C. 20375, USA. (jbishop@uap2.nrl.navy.mil)

J. F. Gómez and C. Morales, Laboratorio de Astrofísica Espacial y Física Fundamental, INTA, Apartado de Correos 50727, E-28080 Madrid, Spain.

E. J. Mierkiewicz and F. L. Roesler, Department of Physics, University of Wisconsin-Madison, 1150 University Avenue, Madison, WI 53706, USA.